Centrum voor Wiskunde en Informatica
REPORT*RAPPORT*

Nonlinear Multigrid for Fully-Implicit and High-Order Accurate Simulation of Multiphase Flow in Porous Media

J. Molenaar

Modelling, Analysis and Simulation (MAS)

MAS-R9712 March 31, 1997

Report MAS-R9712
ISSN 1386-3703

CWI
P.O. Box 94079
1090 GB Amsterdam
The Netherlands

Nonlinear Multigrid for Fully-Implicit and High-Order Accurate Simulation of Multiphase Flow in Porous Media

J. Molenaar
CWI
P.O. Box 94079, 1090 GB Amsterdam, The Netherlands

ABSTRACT

High-order accurate and fully implicit finite difference schemes are widely used for multiphase flow problems. In this paper we analyze the use of point Gauss-Seidel relaxation in a nonlinear multigrid method for the resulting nonlinear systems of equations. Point Gauss-Seidel is unstable for calculating the steady-state of high-order accurate discretizations of the 2D convection equation. Here we present a local Fourier mode smoothing analysis for the transient case. It appears that point Gauss-Seidel is a good smoother provided that the time step is taken small enough. Numerical computations show good multigrid convergence rates for typical test problems.

1991 Mathematics Subject Classification: 65M06, 65M55, 76S05
Keywords and Phrases: nonlinear multigrid, porous medium flow, Gauss-Seidel relaxation
Note: work carried out under project MAS1.3 Porous Media Research

1. Introduction

Many porous media flow problems of practical interest (oil recovery, ground water pollution, etc.) involve several flowing phases. High-order accurate finite difference schemes are widely used for the space discretization of the partial differential equations describing these problems (see e.g. [8],[10]). Especially for compressible flow problems it is attractive to use an implicit scheme for the time integration. This means that we have to solve large systems of nonlinear equations in every time step.

In this paper we consider the use of a nonlinear multigrid method for the iterative solution of these systems of equations. The advantages of this approach are clear: we do not need to compute or store the Jacobian matrix, and (hopefully) the convergence rate does not depend on the mesh size. For the smoothing step of the multigrid algorithm we use point Gauss-Seidel relaxation. Because the linear convection equation is an example of a very simple two-phase flow problem, the suitability of this smoother is not clear. It is well-known that point Gauss-Seidel relaxation is unstable for calculating the steady-state solution of high-order accurate discretizations of the 2D convection equation. For example, in the case of a central discretization, the discretization matrix has zeros on the main diagonal. However, we are not interested in steady states. A local Fourier mode smoothing analysis shows that point Gauss-Seidel is a good smoother for the 2D convection equation provided that the time step is taken small enough.

An outline of this paper is as follows. In Section 2 we state the standard black-oil model, which is a three-phase model (water, oil and gas) with exchange of components. The black-oil

model can be considered as a generic model for compressible multiphase flow. In Section 3 we present a high-order accurate discretization of the black-oil model, which is based on a limited interpolation for the transmissibilities. The classical nonlinear multigrid method is briefly discussed in Section 4. In Section 5 we consider the linear convection model problem. A local Fourier mode analysis is carried out of point Gauss-Seidel relaxation applied to the time implicit discretization of this equation. Some computational results are shown in Section 6, that demonstrate the excellent convergence behavior of the nonlinear multigrid method. More results are reported in [9]. In the final section we summarize some conclusions.

2. Equations

In this section we briefly state the standard black-oil flow model (a more elaborate introduction is found in [1],[4]). The basic equations for multiphase flow in porous media are the continuity equations for all components, and the generalized Darcy laws for all phases. Combining these equations yields the following system of partial differential equations that describe the simultaneous flow of water (w), oil (o) and gas (g):

$$\frac{\partial}{\partial t}\left(\phi\frac{s_{\rm w}}{B_{\rm w}}\right) + q_{\rm w} + \nabla\cdot(kT_{\rm w}(-\nabla p_{\rm w} + \rho_{\rm w}\mathbf{g})) = 0, \tag{2.1}$$

$$\frac{\partial}{\partial t}\left(\phi\frac{s_{\rm o}}{B_{\rm o}}\right) + q_{\rm o} + \nabla\cdot(kT_{\rm o}(-\nabla p_o + \rho_{\rm o}\mathbf{g})) = 0, \tag{2.2}$$

$$\begin{aligned}\frac{\partial}{\partial t}&\left(\phi(\frac{s_{\rm g}}{B_{\rm g}} + R\frac{s_{\rm o}}{B_{\rm o}})\right) + q_{\rm g} + \\ &\nabla\cdot(kT_{\rm g}(-\nabla p_{\rm g} + \rho_{\rm g}\mathbf{g}) + RkT_{\rm o}(-\nabla p_{\rm o} + \rho_{\rm o}\mathbf{g})) = 0.\end{aligned} \tag{2.3}$$

In these equations the phase pressures p_α and the phase saturations s_α are the primary unknowns. $\rho_\alpha(p)$, $B_\alpha(p)$, q_α denote the density, formation volume factor (i.e. the compressibility) and injection/production rate of phase α, respectively, $\mathbf{g}$ the acceleration due to gravity, $R(p)$ the solution gas-oil ratio (i.e. the amount of gas dissolved in oil), k the rock permeability and ϕ the porosity. The transmissibility T_α of phase α is given by

$$T_\alpha(s,p) = \frac{k_{{\rm r}\alpha}(s_)}{B_\alpha(p)\mu_\alpha(p)}, \tag{2.4}$$

where $k_{{\rm r}\alpha}$ denotes the relative permeability and μ_α the phase viscosity. We note that the transmissibilities T_α are given functions of all pressures and saturations, whereas R, B_α, ρ_α and ϕ are functions of the pressures only. To close the system we have the additional relations

$$s_{\rm w} + s_{\rm o} + s_{\rm g} = 1, \tag{2.5}$$

$$p_{\rm o} - p_{\rm w} = p_{\rm ow}, \tag{2.6}$$

$$p_{\rm g} - p_{\rm o} = p_{\rm og}, \tag{2.7}$$

where the capillary pressures $p_{\rm ow}$ and $p_{\rm og}$ are given functions of the saturations. Thus we have obtained a system of three partial differential equations (2.1)-(2.3) and three algebraic relations (2.5)-(2.7) for the six unknowns s_α and p_α.

In addition to these equations we have to specify initial and boundary conditions. Usually no-flow conditions are prescribed at the outer boundaries of the domain, and the difficulties associated with injection or production wells are shifted to the proper modeling of the well terms q_α.

It is standard to use $(s_\mathrm{w}, p_\mathrm{o}, s_\mathrm{g})$ as the set of primary unknowns. However a problem arises if there is locally no free gas present ($s_\mathrm{g} = 0$): the oil is undersaturated with gas. There are basically two approaches in order to deal with this problem. One can reformulate the whole problem and use the component mass fractions as the independent variables. Another possibility is the variable substitution method: if there is no free gas, the solution gas-oil ratio R is used as the primary variable instead of s_g. In this paper we use a variant of the pseudo-gas approach (see [5]) that is especially suited for the multigrid approach that we want to apply.

Let us introduce the pseudo-gas variable s_pg, $s_\mathrm{pg} \in [-s_{\mathrm{pg}0}, +1]$, that is identical to the gas saturation s_g if it is positive, and that is a measure of the amount of gas dissolved in oil if it is negative:

$$s_\mathrm{g} = \max(0, s_\mathrm{pg}) \tag{2.8}$$

$$R(p, s_\mathrm{pg}) = \min\left(1, \frac{s_{\mathrm{pg}0} + s_\mathrm{pg}}{s_{\mathrm{pg}0}}\right) R_\mathrm{m}(p), \tag{2.9}$$

where R_m is the maximum amount of gas the can dissolve in oil at a given pressure p, and $s_{\mathrm{pg}0}$ a positive parameter. By construction the gas accumulation term γ,

$$\gamma(s_\mathrm{w}, p_\mathrm{o}, s_\mathrm{pg}) = \phi\left(\frac{s_\mathrm{g}}{B_\mathrm{g}} + R\frac{s_\mathrm{o}}{B_\mathrm{o}}\right), \tag{2.10}$$

is continuous at $s_\mathrm{pg} = 0$. A simple way to fix $s_{\mathrm{pg}0}$ is to require that the derivative of γ with respect to s_pg is also continuous at $s_\mathrm{pg} = 0$ for a given reference oil saturation $\overline{s}_\mathrm{o}$ and pressure $\overline{p}$, so

$$\lim_{s_\mathrm{pg}\downarrow 0} \frac{\mathrm{d}}{\mathrm{d}s_\mathrm{pg}} \gamma(1 - \overline{s}_\mathrm{o} - s_\mathrm{pg}, \overline{p}, s_\mathrm{pg}) = \lim_{s_\mathrm{pg}\uparrow 0} \frac{\mathrm{d}}{\mathrm{d}s_\mathrm{pg}} \gamma(1 - \overline{s}_\mathrm{o}, \overline{p}, s_\mathrm{pg}). \tag{2.11}$$

Using the Equations (2.8)-(2.11) this condition implies

$$s_{\mathrm{pg}0} = \frac{B_\mathrm{g}(\overline{p})}{B_\mathrm{o}(\overline{p})} \overline{s}_\mathrm{o} R_\mathrm{m}(\overline{p}). \tag{2.12}$$

3. Discretization

In this section we state the standard finite difference discretization for the black-oil model. For ease of notation we only consider the one-dimensional discretization on a grid with uniform mesh width h. The extension of this discretization to nonuniform Cartesian grids in more space dimensions is straightforward. With the usual control volume approach we obtain the space discretized equations

$$\frac{\partial}{\partial t}\left(\phi\frac{s_\mathrm{w}}{B_\mathrm{w}}\right)_i + q_{\mathrm{w},i} + \frac{1}{h}\left((kT_\mathrm{w}\Psi_\mathrm{w})_{i+1/2} - (kT_\mathrm{w}\Psi_\mathrm{w})_{i-1/2}\right) = 0, \tag{3.1}$$

$$\frac{\partial}{\partial t}\left(\phi\frac{s_{\mathrm{o}}}{B_{\mathrm{o}}}\right)_i + q_{\mathrm{o},i} + \frac{1}{h}\left((kT_{\mathrm{o}}\Psi_{\mathrm{o}})_{i+1/2} - (kT_{\mathrm{o}}\Psi_{\mathrm{o}})_{i-1/2}\right) = 0, \tag{3.2}$$

$$\frac{\partial}{\partial t}\left(\phi\frac{s_{\mathrm{g}}}{B_{\mathrm{g}}} + \phi\frac{Rs_{\mathrm{o}}}{B_{\mathrm{o}}}\right)_i + q_{\mathrm{g},i} + \frac{1}{h}\left((kT_{\mathrm{g}}\Psi_{\mathrm{g}} + kRT_{\mathrm{o}}\Psi_{\mathrm{o}})_{i+1/2} - (kT_{\mathrm{g}}\Psi_{\mathrm{g}} + kRT_{\mathrm{o}}\Psi_{\mathrm{o}})_{i-1/2}\right) = 0. \tag{3.3}$$

Here Ψ_α denotes the potential gradient term for phase α,

$$\Psi_\alpha = -\nabla p_\alpha + \rho_\alpha \mathbf{g}, \tag{3.4}$$

the subscript i the discretization cell, and the subscript $i+1/2$ the edge between the cells i and $i+1$. The rock permeability $k_{i+1/2}$ at a cell edge is as usual defined by the harmonic mean

$$k_{i+1/2} = \frac{2k_i k_{i+1}}{k_i + k_{i+1}}, \tag{3.5}$$

and the potential gradient terms Ψ_α are discretized by

$$\Psi_{\mathrm{w}\,i+1/2} = \frac{p_{\mathrm{o}i} - p_{\mathrm{o}i+1} + p_{\mathrm{ow}i+1} - p_{\mathrm{ow}i}}{h} + \frac{\rho_{\mathrm{w}i+1} + \rho_{\mathrm{w}i}}{2} g_x, \tag{3.6}$$

$$\Psi_{\mathrm{o}i+1/2} = \frac{p_{\mathrm{o}i} - p_{\mathrm{o}i+1}}{h} + \frac{\rho_{\mathrm{o}i+1} + \rho_{\mathrm{o}i}}{2} g_x, \tag{3.7}$$

$$\Psi_{\mathrm{g}\,i+1/2} = \frac{p_{\mathrm{o}i} - p_{\mathrm{o}i+1} + p_{\mathrm{og}\,i} - p_{\mathrm{og}\,i+1}}{h} + \frac{\rho_{\mathrm{g}\,i+1} + \rho_{\mathrm{g}\,i}}{2} g_x, \tag{3.8}$$

where g_x is the x-component of the gravity vector.

It is well known that some kind of upwind weighting for the transmissibilities $T_{\alpha\,i+1/2}$ is necessary in order to obtain physically relevant solutions. In conventional simulators a one-point upstream approximation is used:

$$T_{\alpha\,i+1/2} = \begin{cases} T_{\alpha i} & \text{if } \Psi_{\alpha\,i+1/2} \geq 0, \\ T_{\alpha\,i+1} & \text{otherwise.} \end{cases} \tag{3.9}$$

The use of one-point upstream weighting leads to a scheme that is formally first order consistent in space. Although the discrete solutions obtained are physically relevant, they suffer from strong numerical diffusion, i.e., sharp fronts are smeared out. The use of simple second order accurate weighting schemes, like the central scheme and the two-point upstream scheme, causes spurious oscillations near sharp fronts in the solution (see [11]). Accurate solutions without these spurious oscillations are obtained by more complex schemes. These schemes typically involve some kind of nonlinear interpolation for the saturations, fluxes or transmissibilities.

We consider a scheme that is based on a nonlinear interpolation for the transmissibilities $T_{\alpha i}$. Assuming that $\Psi_{\alpha\,i+1/2} \geq 0$, we define

$$T_{\alpha\,i+1/2} = T_{\alpha i} + \frac{1}{2}\psi(r_{\alpha\,i+1/2})(T_{\alpha i} - T_{\alpha\,i-1}), \tag{3.10}$$

where

$$r_{\alpha i+1/2} = \frac{T_{\alpha i+1} - T_{\alpha i}}{T_{\alpha i} - T_{\alpha i-1}}, \tag{3.11}$$

and $\psi(r)$ the so-called limiter function. If we take the limiter function ψ identical to 0, we regain the standard first order upwind scheme. Here we consider the so-called limited κ-schemes (see [7]) that are defined by

$$\psi_\kappa(r) = \begin{cases} 0, & r < 0, \\ 2r, & 0 < r < \frac{1-\kappa}{3-\kappa}, \\ \frac{1-\kappa}{2} + \frac{1+\kappa}{2} r, & \frac{1-\kappa}{3-\kappa} < r < \frac{3+\kappa}{1+\kappa}, \\ 2, & r > \frac{3+\kappa}{1+\kappa}. \end{cases} \tag{3.12}$$

In smooth parts of the solution, where $r \approx 1$, the transmissibilities are then approximated by

$$T_{\alpha i+1/2} = \frac{1+\kappa}{2} \left(\frac{T_{\alpha i} + T_{\alpha i+1}}{2} \right) + \frac{1-\kappa}{2} \left(\frac{-T_{\alpha i-1} + 3T_{\alpha i}}{2} \right). \tag{3.13}$$

So for $\kappa = +1$ this scheme is equivalent to the central scheme in smooth parts of the solution, and for $\kappa = -1$ it is equivalent to the two-point upstream scheme. The limited $\kappa = -1$ scheme is equivalent to the classical two-point upstream scheme (see [11]) with the constraints

$$\min\left(T_{\alpha i}, T_{\alpha i+1}\right) \leq T_{\alpha i+1/2} \leq \max\left(T_{\alpha i}, T_{\alpha i+1}\right). \tag{3.14}$$

Moreover, the choice $\kappa = 1/3$ is of special interest: the discretization of the linear convection equation on a uniform orthogonal grid is third order accurate. However, this does not imply that the discretization of the full problem (3.1)-(3.3) is third order accurate.

Analogous to the interpolation of the transmissibilities in Equation (3.10), we use a limited interpolation for the gas-oil ratio $R_{i+1/2}$. If the interpolation of the transmissibilities $T_{\alpha i+1/2}$ and the gas-oil ratio $R_{i+1/2}$ is at least second order accurate in smooth parts of the solution, this implies that the whole scheme is formally second order consistent in space. So far we have not discussed the time integration method. Use of the implicit Euler method yields the standard fully implicit formulation, that is unconditionally stable, but only first order consistent in time. Second order consistency is obtained by using the trapezoidal rule (i.e., the Crank-Nicholson scheme), which is only slightly more expensive than the implicit Euler method.

4. Multigrid Method

In this section we briefly discuss the cell-centered nonlinear multigrid method that we use. Suppose that on the fine grid we have the system of equations

$$\mathcal{N}^h(u^h) = f^h, \tag{4.1}$$

where $\mathcal{N}^h$ is a nonlinear operator. The coarse grid corrections that we consider are of the form

$$\mathcal{N}^{2h}(\tilde{u}^{2h}) = \mathcal{N}^{2h}(u^{2h}) + \overline{R}^h_{2h}(f^h - \mathcal{N}^h(u^h)), \tag{4.2}$$

$$\tilde{u}^h = u^h + P^{2h}_h(\tilde{u}^{2h} - u^{2h}). \tag{4.3}$$

Here $\overline{R}_{2h}^{h}$ and P_h^{2h} denote the restriction of the residual, and the prolongation of the correction, respectively. We take $\overline{R}_{2h}^{h}$ to be the adjoint of the interpolation by a piecewise constant function. In cell-centered multigrid methods this is natural: the residual (the total excess of accumulation and net flow) in a coarse grid cell, is the sum of the residuals in the corresponding fine grid cells. The prolongation P_h^{2h} is a piecewise linear interpolation. This combination of prolongation and restriction is formally sufficiently accurate to deal with second order partial differential equations.

To obtain the coarse grid operator $\mathcal{N}^{2h}$, the problem is discretized on the coarse grid, i.e., a grid with mesh size $2h$. However, we do not use the same discretization on all grids. Only on the finest grid we use the high-order accurate discretization with the interpolated transmissibilities as given by Equation (3.10). On the coarser grids we use the standard one-point upstream discretization (see (3.9)). Because the problem is nonlinear, the properties of the coarse grid operators are determined by the choice of u^{2h}. We take

$$u^{2h} = R_{2h}^{h} u^{h}, \tag{4.4}$$

where R_{2h}^{h} is again the adjoint of interpolation by a piecewise constant function.

5. Local Fourier Mode Analysis for Point Gauss-Seidel

The choice of a robust smoother is of prime importance for any good multigrid algorithm. Neglecting compressibility and capillary effects, the multiphase flow equations that we consider are of mixed elliptic-hyperbolic type. The convergence analysis of smoothers for elliptic equations is well developed. However the convergence analysis for first order hyperbolic equations is less complete.

In this section we study the convergence behavior of point Gauss-Seidel relaxation for the linear convection equation, that is discretized with a κ-scheme. The linear convection equation is obtained for the incompressible two-phase flow model, if we take $T_{\mathrm{w}}(s_{\mathrm{w}}) = s_{\mathrm{w}}$. This study is of interest because it is well-known that point Gauss-Seidel relaxation is not suitable for the calculation of the *steady state* of two-dimensional problems. In [6] it is shown that for the case $\kappa = 1/3$ some high frequency error modes are amplified when it is applied in a sweep direction different from the upstream direction. In addition, we remark that some *low* frequency error modes are amplified when point Gauss-Seidel relaxation is applied in the upstream direction.

However, we are not really interested in steady state computations, but in time accurate implicit calculations. We expect that this error amplification does not occur if sufficiently small time steps are taken. To proof this we consider the backward Euler time integration, and carry out a local Fourier mode analysis.

For simplicity we first consider the one-dimensional case. The model problem that we consider is

$$\frac{\partial u}{\partial t} + v \frac{\partial u}{\partial x} = 0, \tag{5.1}$$

where v is the flow velocity. The discretization of this equation with a linear κ-scheme

$(-1 \leq \kappa \leq 1)$ can be written as

$$u_i^n = u_i^{n+1} + \frac{\lambda}{4}\left((1-\kappa)u_{i-2}^{n+1} + (3\kappa-5)u_{i-1}^{n+1} + (3-3\kappa)u_i^{n+1} + (1+\kappa)u_{i+1}^{n+1}\right), \tag{5.2}$$

where $\lambda = v\Delta t/\Delta x$ denotes the CFL-number.

In one space dimension point Gauss-Seidel relaxation can be performed in two directions: the downstream direction (indicated by $\nearrow$), the upstream direction ($\swarrow$). Let $\hat{S}_\kappa^*(\omega,\lambda)$ be the Fourier symbol of the error amplification operator of point Gauss-Seidel in a given direction, then

$$\hat{S}_\kappa^* = 1 - \frac{\hat{L}_\kappa}{\hat{\tilde{L}}_\kappa^*}, \tag{5.3}$$

where $\hat{L}_\kappa$ is the Fourier symbol of the linear operator defined by the right hand side of Equation (5.2),

$$\hat{L}_\kappa = 1 + \frac{\lambda}{4}((1-\kappa)e^{-2i\omega} + (3\kappa-5)e^{-i\omega} + (3-3\kappa) + (1+\kappa)e^{i\omega}), \tag{5.4}$$

and $\hat{\tilde{L}}_\kappa^*$ the Fourier symbol of the approximation to it (see e.g. [3]). For the downstream direction we have

$$|\hat{S}_\kappa^{\nearrow}| = \frac{1+\kappa}{|4\lambda^{-1} + 3 - 3\kappa + (1-\kappa)e^{-2i\omega} + (3\kappa-5)e^{-i\omega}|}, \tag{5.5}$$

and the maximum error amplification factor occurs for the low frequency Fourier mode $\omega = 0$:

$$\sup_{\omega\in(-\pi,\pi)} |\hat{S}_\kappa^{\nearrow}(\omega,\lambda)| = |\hat{S}_\kappa^{\nearrow}(0,\lambda)| = \frac{1+\kappa}{|4\lambda^{-1} - 1 - \kappa|}. \tag{5.6}$$

For $\lambda = 4/(1+\kappa)$ the low frequency error mode $\omega = 0$ is blown up by the point Gauss-Seidel relaxation! However, if we take $\lambda \ll 4/(1+\kappa)$, so a small time step, point Gauss-Seidel is an efficient iterative solver, and a fortiori a good smoother. Point Gauss-Seidel applied in the downstream direction is of course a direct solver for the two-point downstream scheme $(\kappa = -1)$.

For the upstream direction we have

$$\sup_{\omega\in(-\pi,\pi)} |\hat{S}_\kappa^{\swarrow}(\omega,\lambda)| = |\hat{S}_\kappa^{\swarrow}(\pi,\lambda)| = \frac{6-4\kappa}{|4\lambda^{-1} + 2 - 4\kappa|}. \tag{5.7}$$

Blow up of high frequency error modes now occurs if $\lambda = 2/(2\kappa-1)$. If $\kappa < 1/2$ the error amplification factor $|\hat{S}_\kappa^{\swarrow}(\pi,\lambda)|$ is always bounded.

This 1D example shows that point Gauss-Seidel is a good smoother if the time step is small enough, and the blow up of Fourier error modes may occur if the time step is too large. Let us next consider the two-dimensional case that is of more practical relevance.

The 2D linear convection equation is given by

$$\frac{\partial u}{\partial t} + v\left(\cos\beta\frac{\partial u}{\partial x} + \sin\beta\frac{\partial u}{\partial y}\right) = 0, \quad 0 \leq \beta < \frac{\pi}{2}, \tag{5.8}$$

where β denotes the angle between the flow velocity and the x-axis. In two space dimensions point Gauss-Seidel relaxation can be performed in four directions: the downstream direction the upstream direction and two cross-stream directions, indicated by $\searrow$ and $\nwarrow$. As before $\hat{S}^*_\kappa(\omega_x, \omega_y, \beta, \lambda)$ denotes the Fourier symbol of the error amplification operator of point Gauss-Seidel in a given direction. We say that point Gauss-Seidel relaxation is bounded if no Fourier error mode is blown up in the point Gauss-Seidel relaxation for any flow angle β.

Definition 1 *Point Gauss-Seidel relaxation in a given sweep direction is called* conditionally bounded *if there exists a* $\overline{\lambda}$ *such that*

$$\sup_{\beta\in[0,\frac{\pi}{2})}\sup_{(\omega_x,\omega_y)\in[-\pi,\pi]^2}|\hat{S}_\kappa(\omega_x,\omega_y,\beta,\lambda)|<\infty,\quad\forall\lambda<\overline{\lambda}. \tag{5.9}$$

A point Gauss-Seidel sweep is called unconditionally bounded *if*

$$\sup_{\beta\in[0,\frac{\pi}{2})}\sup_{(\omega_x,\omega_y)\in[-\pi,\pi]^2}|\hat{S}_\kappa(\omega_x,\omega_y,\beta,\lambda)|<\infty,\quad\forall\lambda\geq 0. \tag{5.10}$$

In the following lemma's we study the boundedness of point Gauss-Seidel relaxation in two space dimensions for the four possible relaxation directions, and derive values for $\overline{\lambda}$ depending on κ. Because $\overline{\lambda}$ is an upper bound for λ, it determines an upper bound for the time step Δt.

Lemma 1 *Point Gauss-Seidel in the downstream direction* ($\nearrow$) *is unconditionally bounded for* $\kappa=-1$*, and conditionally bounded for* $\kappa\in(-1,1]$ *with*

$$\overline{\lambda}\leq\frac{2\sqrt{2}}{\kappa+1}. \tag{5.11}$$

Proof It is sufficient to consider the cases that

$$\hat{\tilde{L}}^{\nearrow}_\kappa(\omega_x,\omega_y,\beta)=0. \tag{5.12}$$

For the downstream direction we have

$$\begin{aligned}\hat{\tilde{L}}^{\nearrow}_\kappa &= 1+\lambda(3-3\kappa)(\cos\beta+\sin\beta)/4+\\ &\quad\lambda\cos\beta((1-\kappa)e^{-2i\omega_x}+(3\kappa-5)e^{-i\omega_x})/4+\\ &\quad\lambda\sin\beta((1-\kappa)e^{-2i\omega_y}+(3\kappa-5)e^{-i\omega_y})/4.\end{aligned}$$

Because

$$\min_{\omega\in[0,2\pi)}\Re\left((1-\kappa)e^{-2i\omega}+(3\kappa-5)e^{-i\omega}\right)=-4+2\kappa, \tag{5.13}$$

for $-1\leq\kappa\leq 1$, it follows that

$$\Re\left(\hat{\tilde{L}}^{\nearrow}_\kappa\right)\geq 1-\frac{1+\kappa}{4}\lambda\sqrt{2}. \tag{5.14}$$

Condition (5.11) is necessary, because

$$\hat{\tilde{L}}^{\nearrow}_\kappa(0,0,\frac{\pi}{4},\frac{2\sqrt{2}}{\kappa+1})=0, \tag{5.15}$$

and

$$\hat{L}_\kappa(0,0,\frac{\pi}{4},\frac{2\sqrt{2}}{\kappa+1}) = \lambda\frac{1+\kappa}{4}\sqrt{2}. \tag{5.16}$$

For $\kappa = -1$ we have $\hat{L}_\kappa = \hat{\tilde{L}}_\kappa^{\nearrow}$. Hence point Gauss-Seidel in the downstream direction is an exact solver, and as a matter of course unconditionally bounded. ∎

Lemma 2 *Point Gauss-Seidel in the upstream direction ($\swarrow$) is unconditionally bounded for $\kappa \in [-1, 1/2)$, and conditionally bounded for $\kappa \in [1/2, 1]$ with*

$$\overline{\lambda} = \frac{\sqrt{2}}{2\kappa - 1}. \tag{5.17}$$

PROOF Consider the real part of $\hat{\tilde{L}}_\kappa^{\swarrow}$:

$$\begin{aligned}
\Re(\hat{\tilde{L}}_\kappa^{\swarrow}) &= \Re(1 + \lambda\cos\beta(3 - 3\kappa + (1+\kappa)e^{i\omega_x})/4 + & (5.18)\\
&\qquad \lambda\sin\beta(3 - 3\kappa + (1+\kappa)e^{i\omega_y})/4) \\
&\geq 1 + \lambda(1-2\kappa)(\sin\beta + \cos\beta)/2 & (5.19)\\
&\geq 1 + \lambda\frac{1-2\kappa}{2}\sqrt{2}. & (5.20)
\end{aligned}$$

Condition (5.17) is necessary for $(\omega_x, \omega_y) = (\pi, \pi)$, $\beta = \pi/4$ and $\lambda = \overline{\lambda}$. ∎

Finally we derive a necessary condition for boundedness in the case of cross-stream relaxation. We only have to consider one sweep direction, because the two cross-stream directions are equivalent by the transformation $\beta \to \pi/2 - \beta$.

Lemma 3 *Point Gauss-Seidel in the cross-stream direction is unconditionally bounded for $\kappa = -1$, and conditionally bounded for $-1 < \kappa \leq 1$, with*

$$\overline{\lambda} = \begin{cases} 4/(\kappa+1), & -1 < \kappa < 1/2, \\ 4/\sqrt{17\kappa^2 - 14\kappa + 5}, & 1/2 < \kappa \leq 1. \end{cases} \tag{5.21}$$

PROOF For the real part of $\hat{\tilde{L}}_\kappa^{\nwarrow}$ we have

$$\begin{aligned}
\Re(\hat{\tilde{L}}_\kappa^{\nwarrow}) &= 1 + \Re\left(\lambda\cos\beta(3 - 3\kappa + (3\kappa-5)e^{-i\omega_x}(1-\kappa)e^{-2i\omega_x})/4 + \right. \\
&\qquad \left. \lambda\sin\beta(3 - 3\kappa + (1+\kappa)e^{i\omega_y})/4\right) \\
&\geq 1 + \frac{-1-\kappa}{4}\lambda\cos\beta + \frac{2-4\kappa}{4}\lambda\sin\beta,
\end{aligned}$$

so condition (5.21) is sufficient for boundedness. Moreover it is a necessary condition as can be seen by substituting $(\omega_x, \omega_y) = (0, \pi)$, $\lambda = \overline{\lambda}$, and

$$\beta = \max(0, \operatorname{atan}((\kappa+1)/(4\kappa-2))).$$

For $\kappa = -1$ we have

$$\begin{aligned} \left|\hat{S}_\kappa^{\nwarrow}(\omega_x,\omega_y,\beta,\lambda)\right| &= \left|\frac{\cos\beta(2e^{-2i\omega_x}-8e^{-i\omega_x})}{4\lambda^{-1}+6\cos\beta+\sin\beta(2e^{-2i\omega_y}-8e^{-i\omega_y}+6)}\right| \\ &\leq \left|\frac{10\cos\beta}{4\lambda^{-1}+6\cos\beta}\right| \leq \frac{5}{3}, \end{aligned} \tag{5.22}$$

which shows the unconditional boundedness. ∎

In practice the flow angle β is not a priori known, and therefore we apply point Gauss-Seidel in all four directions. If we want to avoid blow-up of any Fourier mode in each of the four possible sweep directions, this poses the following condition on λ.

Theorem 1 *The maximum value for λ that gives boundedness of point Gauss-Seidel relaxation for all four sweep directions is given by*

$$\lambda = \frac{2\sqrt{2}}{\kappa+1}. \tag{5.23}$$

Proof Follows from Lemma 1,2 and 3. ∎

We note that point Gauss-Seidel for the two-point upstream scheme ($\kappa = -1$) is not only an exact solver when applied in the downstream direction, but it is also unconditionally bounded for the other three sweep directions.

So far we have only considered the boundedness of $\hat{S}_\kappa(\omega_x,\omega_y,\beta,\lambda)$. Of course we are really interested in the convergence behavior. Therefore we consider the convergence rate $\overline{\rho}_\kappa(\beta,\lambda)$ for all Fourier modes, and the smoothing factor $\rho_\kappa(\beta,\lambda)$ for the high frequency Fourier modes,

$$\rho_\kappa(\beta,\lambda) = \sup_{(\omega_x,\omega_y)\in[-\pi,\pi]^2/[-\pi/2,\pi/2]^2} \left|\hat{S}_\kappa^{\swarrow}\hat{S}_\kappa^{\nearrow}\hat{S}_\kappa^{\searrow}\hat{S}_\kappa^{\nwarrow}\right|^{1/4}. \tag{5.24}$$

For $\kappa = -1$ four direction point Gauss-Seidel is a direct solver, so $\rho_{-1} = \overline{\rho}_{-1} = 0$. For other values of κ we have to approximate ρ_κ and $\overline{\rho}_\kappa$ numerically. Here we only consider the case $\kappa = 1/3$, because it leads to a third order accurate scheme. Other values for κ give second order accurate schemes, and it that case we prefer $\kappa = -1$. On uniform grids with $\Delta x = \Delta y$ the maximal step for $\kappa = 1/3$ schemes is determined by

$$\Delta t < \frac{3\Delta x}{v\sqrt{2}}. \tag{5.25}$$

In Fig. 6.1 ρ and $\overline{\rho}$ are shown for $\kappa = 1/3$ and $\beta = \pi/4$. This choice for the flow angle β yields the worst smoothing factors. We observe that four direction point Gauss-Seidel relaxation is a good smoother for the $\kappa = 1/3$ scheme if $\lambda < 2$.

6. Numerical Examples

Let us now study the behavior of our multigrid algorithm for two test problems. The first test problem is a one-dimensional black-oil test problem for which a reliable reference solution is available. It involves compressibility effects and the dissolution of gas in oil. The second test problem models the water flooding of the quarter of a five spot pattern.

Table 6.1: Average multigrid convergence rate on different grids for gravity inversion problem.

	30	60	120	180
1-point upstream	0.23	0.27	0.28	0.29
2-point upstream	0.37	0.45	0.51	>1.0
3-rd order accurate	0.29	0.30	0.30	0.32

In our numerical experiments we use the second order accurate Crank-Nicholson scheme for the time integration. The time step is chosen adaptively, such that the changes in the water saturation and the pseudo-gas saturation are approximately Δs:

$$\Delta t^{n+1} = \frac{\Delta s}{\|{s_\alpha}^n - {s_\alpha}^{n-1}\|_\infty} \Delta t^n, \quad \alpha = \mathrm{w}, \mathrm{pg}. \tag{6.1}$$

In our calculations we take $\Delta s = 0.01$. The ratio $\Delta t^{n+1}/\Delta t^n$ is bounded between 0.5 and 2.0. The resulting system of nonlinear equations is solved by multigrid iteration. In any time step the initial residual is reduced by a factor of 10^{-5} by means of a number of F-cycles. For relaxation we use symmetric Gauss-Seidel relaxation in 1D, and four direction Gauss-Seidel relaxation in 2D. The different sweeps are divided over the pre- and post smoothing step. On the coarsest grid in the calculation the discrete problem is solved exactly.

6.1 Problem 1

The first test problem is a one-dimensional gravity inversion problem taken from [2]. The column is 100 ft in length and is capped with no flow boundaries at each end. Initially the lower part is filled with free gas, the middle part with pure oil, and the upper part with pure water. The fluids start to flow because of gravity, and there is dissolution of gas in the oil phase. In Fig. 6.2 the numerical solution on a grid with 120 points is shown for the one-point upstream scheme (top), the limited (see (3.12)) $\kappa = -1$ scheme (middle) and the $\kappa = 1/3$ scheme (bottom). The left column shows the solution at roughly 60 days and the right column the solution at 120 days. We observe that the solution obtained by the limited two-point upstream scheme is completely different from the other two solutions: it has a single shock in the gas saturation. Using smaller time steps, i.e., a smaller value for Δs, does not change this result. Because the other two solutions are in good qualitative agreement with the solution reported in [2], we conclude that this is unphysical. The $\kappa = 1/3$ scheme gives a good resolution of the solution. Notice the 'gas bubble' at the water front.

The average convergence rate over all time steps for multigrid F-cycles is shown in Table 6.1. We do not find any superior convergence behavior for the two-point upstream scheme: it diverges on the grid with 180 points. We observe a nearly equal convergence behavior for the one-point upstream and the $\kappa = 1/3$ scheme. There is no penalty in the sense of multigrid convergence behavior for the improved accuracy.

6.2 Problem 2

In this two-dimensional example we model the water flooding of the quarter of a five spot pattern. A small compressibility of water and oil is taken into account. The data are taken

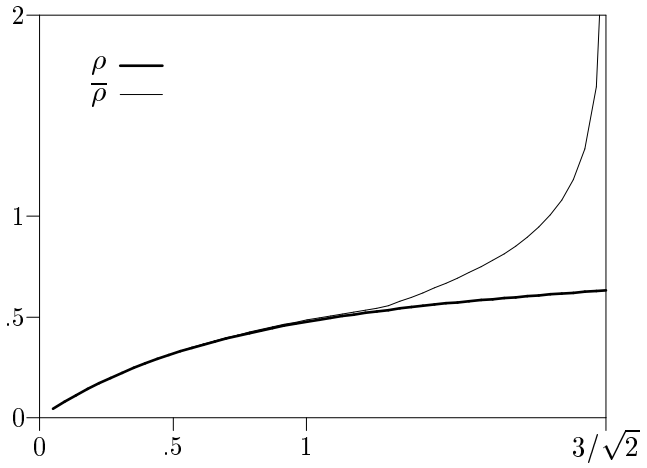

Figure 6.1: Plot of the smoothing rate ρ and the error amplification factor $\overline{\rho}$ for $\kappa = 1/3$ and $\beta = \pi/4$.

Table 6.2: Simulation statistics for quarter of a five-spot pattern problem.

	20×20	40×40	80×80
Average convergence rate	0.01	0.02	0.03
Time steps	79	117	200
CPU sec (SGI-Indy)	50	365	4420

from [10]. In Fig. 6.3 a contour plot of the water saturation is shown for the one-point upstream scheme, and the $\kappa = 1/3$ scheme. The contour lines are drawn at equidistant levels of 0.1. As expected, the $\kappa = 1/3$ scheme gives a superior resolution of the shock. Some statistical data for the $\kappa = 1/3$ calculation are shown in Table 6.2. The CPU times needed for the calculations on different grids are reported for a SGI-Indy works station with a 100 MHz CPU. The convergence of the multigrid algorithm is very fast. This is due to the fact that the pressure field is nearly constant. It is only coupled to the saturation distribution by small differences in the oil and water compressibility. As shown in the previous section, the point Gauss-Seidel relaxation is a very efficient solver for the transport part of the equations.

7. Conclusions

We have developed a high-order accurate and fully-implicit discretization of the black-oil model. This black-oil model is a generic model for compressible multiphase flow. For the solution of the discretized equations we used a multigrid algorithm with a point Gauss-Seidel smoother. A local Fourier mode analysis has been presented for the high-order accurate discretization of the linear convection equation. Upper bounds on the time step have been derived that ensure boundedness of the Gauss-Seidel iteration. Surprisingly there is no upper

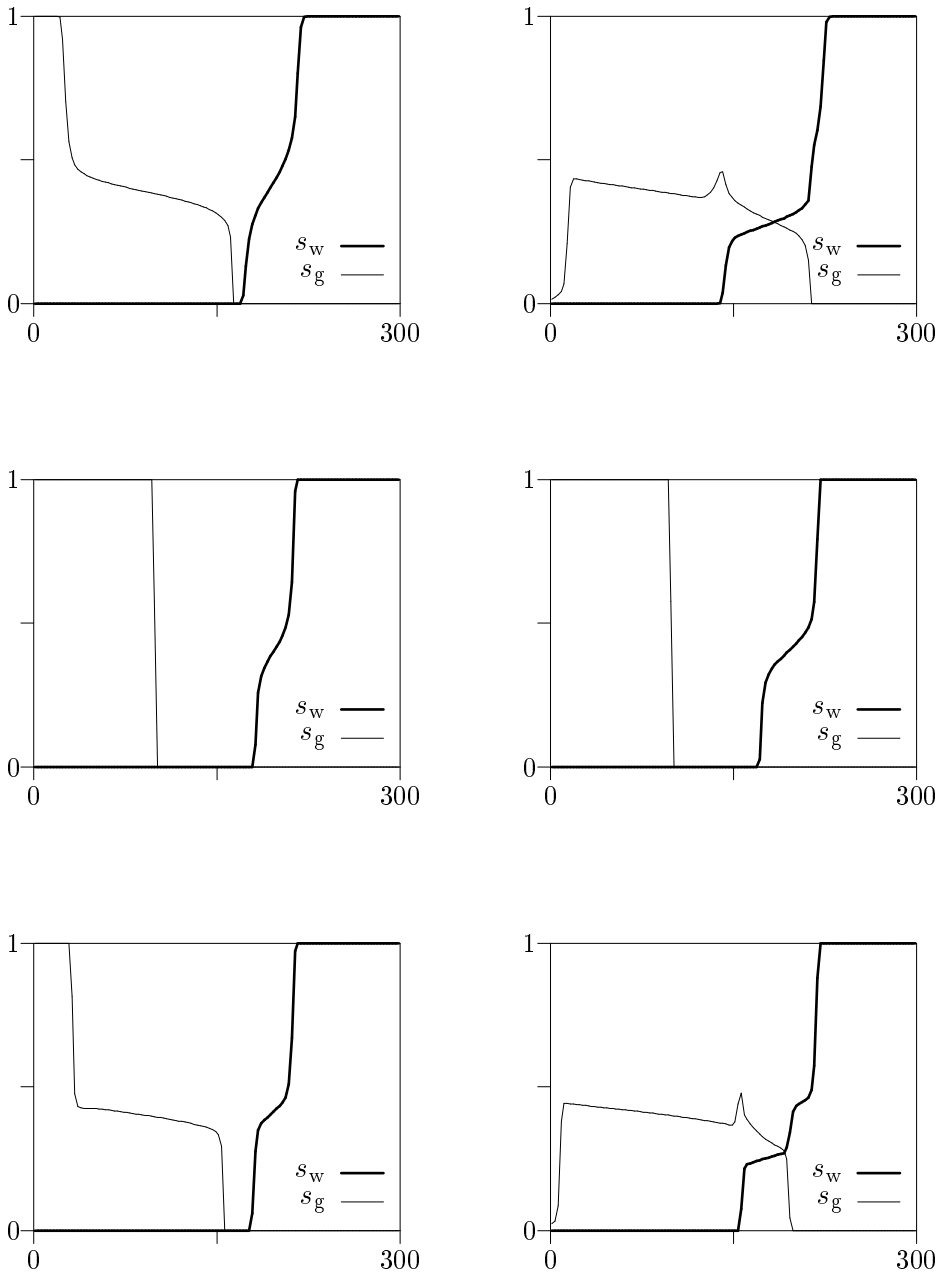

Figure 6.2: Numerical solution of gravity inversion problem for three different discretizations: one-point upstream, two-point upstream and third order accurate interpolation.

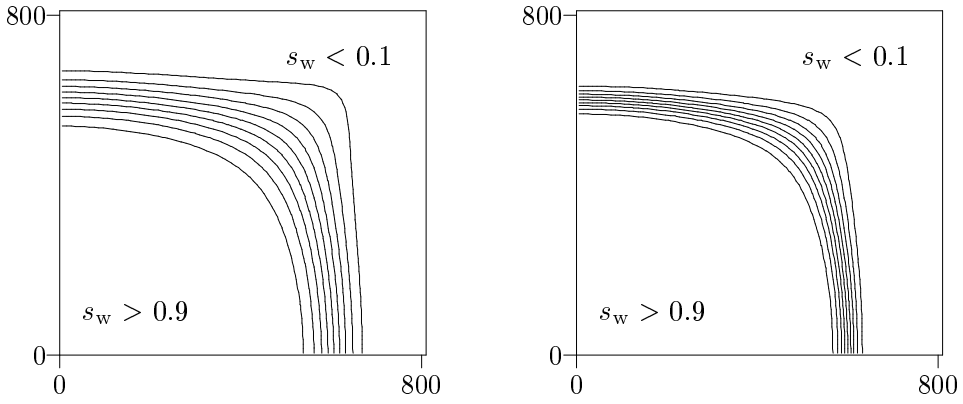

Figure 6.3: Contour plot of the water saturation in water flooding of the quarter of a five spot pattern: one-point upstream (left) and $\kappa = 1/3$ (right).

bound for the two-point upstream scheme: besides being an exact solver when applied in the downstream direction, there is no blow up of Fourier modes when it is applied in other directions. Sample calculations for typical multiphase flow problems demonstrate the suitability of the multigrid approach: the convergence is fast and grid independent. A limited two-point upstream scheme converges to an unphysical solution, and we do not observe any superior multigrid convergence behavior for this scheme.

References

1. K. Aziz and A. Settari. *Petroleum Reservoir Simulation.* Elsevier Applied Science Publishers, 1979.
2. J.B. Bell, P. Colella, and J.A. Trangenstein. Higher order Godunov methods for general systems of hyperbolic conservation laws. *J. Comput. Phys.*, 82:362–397, 1989.
3. A. Brandt. Guide to multigrid development. In W. Hackbusch and U. Trottenberg, editors, *Multigrid Methods, Lecture Notes in Mathematics*, pages 220–312, Berlin, 1982. Springer-Verlag.
4. L.P. Dake. *Fundamentals of reservoir engineering.* Elsevier, 1978.
5. P. Forsyth Jr. and P.H. Sammon. Gas phase appearance and disappearance in fully implicit black oil simulation. *Soc. Pet. Eng. J.*, 24:505–507, 1984.
6. B. Koren. *Multigrid and Defect Correction for the Steady Navier-Stokes Equations, An Application to Aerodynamics.* Centre for Mathematics and Computer Science, Amsterdam, 1990. CWI-tract 74.
7. B. van Leer. Upwind difference methods for aerodynamic problems governed by the Euler equations. In B.E. Engquist, S. Osher, and R.C.J. Sommerville, editors, *Large*

Scale Computations, part 2, Lectures in Applied Mathematics, pages 327–336. American Mathematical Society, Providence, Rhode Island, 1985.

8. J. Liu, G.A. Pope, and K. Sepehrnoori. High-resolution, fully implicit method for enhanced oil recovery simulation. *SPE 29098*, 1995. 13th Symposium on Reservoir Simulation, San Antonio.
9. J. Molenaar. Multigrid methods for high-order accurate fully implicit simulation of flow in porous media. In J.-A. Désidéri, P. Le Tallec, E. Onate, J. Périaux, and E.Stein, editors, *Proceedings of the Second ECCOMAS Conference on Numerical Methods in Engineering*, pages 291–297. John Wiley, 1996.
10. B. Rubin and M.J. Blunt. Higher-order implicit flux limiting schemes for black-oil simulation. *SPE 21222*, 1991. SPE Reservoir Simulation Symposium, Anaheim.
11. M.R. Todd, P.M. O'Dell, and G.J. Hirasaki. Methods for increased accuracy in numerical reservoir simulators. *Soc. Pet. Eng. J.*, 12:515–530, 1972.